http://dx.doi.org/10.5012/bkcs.2014.35.7.2072

Electrodeposition of Gold on Fluorine-Doped Tin Oxide: Characterization and Application for Catalytic Oxidation of Nitrite

Md. Mahbubur Rahman, Xiao-Bo Li, Nasrin Siraj Lopa, and Jae-Joon Lee*

*Nanotechnology Research Center & Department of Applied Life Science, College of Biomedical and Health Science, Konkuk University, Chungju 380-701, Korea. *E-mail: jjlee@kku.ac.kr*
Received January 7, 2014, Accepted March 17, 2014

Sub-micrometer size gold particles were electrodeposited on a transparent fluorine-doped tin oxide (FTO) from acetonitrile solution containing $AuCl_4^-$ and tetramethylammonium tetraflouroborate (TMATFB) for detecting NO_2^-. A series of two-electron ($2e^-$) and one-electron ($1e^-$) reductions of the $AuCl_4^-$-$AuCl_2^-$-Au redox systems were observed at FTO and a highly stable and homogeneous distribution of Au on FTO (Au/FTO) was obtained by stepping the potential from 0 to −0.55 V (*vs.* Ag/Ag^+). The Au/FTO electrode exhibited sufficiently high catalytic activity toward the oxidation of NO_2^- with a detection limit (*S/N* = 3) and sensitivity of 2.95 μM and 223.4 $\mu A \cdot cm^{-2} \cdot mM^{-1}$, respectively, under optimal conditions. It exhibited an interference-free signal for NO_2^- detection with excellent recoveries from real samples.

Key Words : Gold, Fluorine-doped tin oxide, Electrodeposition, Cyclic voltammetry, Nitrite oxidation

Introduction

Electrodes modified with gold nanostructures have attracted much interest because of their stability and high surface area along with an excellent catalytic activity toward many analytes including CO and nitrite (NO_2^-).[1-3] They are particularly suitable for many electrochemical sensor applications such as the quantitative detection of NO_2^- level in many foods and human blood stream to facilitate compliance with the maximum contaminant level of NO_2^- (MCL; 1 ppm, 21.7 μM, as defined by the Environmental Protection Agency (EPA)).[4-7]

Although the electrochemical detection method is simple and cost-effective,[8-10] it often requires undesirably high overvoltage for voltammetric oxidation/reduction of NO_2^-, which in turn causes significant interference by other readily oxidized compounds (*e.g.*, Ca^{2+}, Zn^{2+}, Cl^-, SO_4^{2-}, NO_3^-, *etc.*).[11] Therefore, the preparation of electrodes modified by Au would be a promising strategy to decrease the oxidation/reduction overpotential[12] for many applications that require high catalytic activities at electrodes; it would also be very useful when thin and transparent conducting oxides (TCOs) are used as substrates for electrode preparation. TCOs such as indium tin oxide (ITO) and fluorine-doped tin oxide (FTO) are already used in a wide variety of applications for biosensors, display devices, and many solar energy conversion systems.[13-15] Although various self-assembly approaches have been applied to the deposition of gold nanostructures on TCOs, they usually require special organic binders such as (aminopropyl)siloxane, (mercaptopropyl)siloxane,[16] which often deteriorate the catalytic activity and conductivity of Au deposits. Meanwhile there were many reports on the electrodeposition of Au directly on ITO in an aqueous phase,[17-19] it was hardly found on FTO even though the latter is more useful in many cases where higher thermal and chemical stabilities are required. Sheridan *et al.* directly electrodeposited Au nanoparticles on FTO and 3-aminopropyldimethylmethoxysilane (ADMMS)-modified FTO in an aqueous phase with an emphasis on the control of nucleation mechanism,[20] while the potential application to sensing devices were left for further study.

This work reports a similar binder-free approach for the electrochemical deposition of sub-micrometer size Au particles on FTO at room temperature from acetonitrile solution to investigate the catalytic oxidation of NO_2^-. It was found that the Au/FTO electrode prepared in this study performed a strong catalytic oxidation of NO_2^- within a reasonable detection range without any serious interference from many common ions.

Experimental

Chemicals. Double-distilled water obtained from a Milli-Q water-purifying system (18 MΩ·cm) was used in all experiments. Chloroauric acid ($HAuCl_4$), acetonitrile, tetramethylammonium tetraflouroborate (TMATFB), disodium hydrogen phosphate (Na_2HPO_4), sodium dihydrogen phosphate (NaH_2PO_4), sodium nitrite ($NaNO_2$), calcium chloride ($CaCl_2$), magnesium sulfate ($MgSO_4$), zinc chloride ($ZnCl_2$), zinc nitrate ($Zn(NO_3)_2$), and sodium carbonate (Na_2CO_3) were used as received from Sigma-Aldrich. Phosphate buffer saline (PBS) solution was prepared by mixing 0.1 M Na_2HPO_4 with 0.1 M NaH_2PO_4.

Instrumentation. A CHI430A electrochemical workstation (CH instruments, Inc. USA) was used for electrochemical measurements. An FTO electrode (8 Ω/Sq. TEC8, Pilkington), a platinum wire, and a Ag/Ag^+ or Ag/AgCl (*aq*, saturated KCl) electrode were used as working, counter, and reference electrodes, respectively. Differential pulse voltammograms (DPVs) were obtained by scanning the potential from 0.6 to

1.0 V with the pulse amplitude of 100 mV·s^{-1}, pulse width of 2 ms, and pulse period of 100 ms. Electrochemical impedance spectra (EIS) were obtained at +0.30 V in the frequency range of 10^5-0.1 Hz with an AC amplitude of 5 mV (IM6ex, Zahner-Elektrik GmbH & Co. KG). Simulation of EIS spectra with the equivalent circuit model was performed by using Z-view software (version 3.1, Scribner Associates Inc., USA). Field emission scanning electron microscopy (FE-SEM, JSM-6700F, JEOL) and energy dispersive X-ray spectroscopy (EDS, INCAx-sight7421, Oxford Instruments) were used to characterize the surface morphology and elements, respectively.

Deposition of Gold on FTO. A sheet of FTO (15 × 30 mm^2) was cleaned by sonication in Triton X-100 aqueous solution and washed with ethanol and acetone followed by drying under nitrogen purging. For the electrochemical deposition of Au, the FTO sheet was placed into a Teflon cell containing acetonitrile with 0.5 mM $HAuCl_4$ and 0.25 mM TMATFB. The cell had an exposed area of *ca.* 0.32 cm^2 defined by O-ring. Au/FTO was prepared by stepping the potential from 0 to −0.55 V for 25, 50, or 100 s.

Results and Discussion

Redox Behavior of $AuCl_4^-$ at FTO. In Figure 1, two cathodic waves are observed at *ca.* −0.30 (I) and −0.65 V (II) in the cyclic voltammograms (CVs) of $AuCl_4^-$ at FTO during a negative potential scan from 2.0 to −0.75 V along with the corresponding anodic waves that peak at *ca.* 1.5 (I') and 0.67 V (II') in the reverse scan. They are attributed to the reduction of $AuCl_4^-$ to $AuCl_2^-$, and of $AuCl_2^-$ to Au (*i.e.*, the forward reactions of 1 and 2), respectively, while the two corresponding anodic peaks are assigned to I' and II' (*i.e.*, the backward reactions of 1 and 2), respectively.[21]

$$AuCl_4^- + 2e^- \leftrightarrow AuCl_2^- + 2Cl^- \quad (1)$$

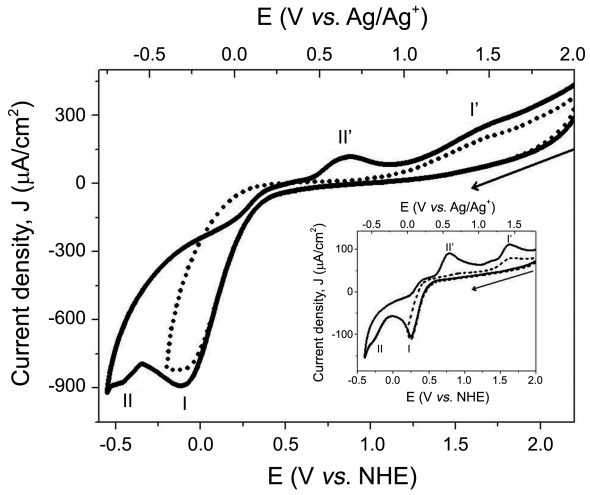

Figure 1. Cyclic voltammograms (CVs) obtained at an FTO electrode in an acetonitrile solution containing 0.5 mM $HAuCl_4$ and 0.25 mM TMATFB. Potential scan range: 2.0 to −0.75 V (solid line); 2.0 to −0.40 V (dot line). Inset shows CVs obtained at GCE in the same solution. Potential scan range: 2.0 to −0.75 V (solid line); 2.0 to −0.40 V (dash line). Scan rate: 100 mV·s^{-1}.

$$AuCl_2^- + e^- \leftrightarrow Au + 2Cl^- \quad (2)$$

Similar voltammetric behavior of $AuCl_4^-$ was observed at a glassy carbon electrode (GCE) (Inset, Fig. 1) and is essentially consistent with the voltammetric responses of $AuCl_4^-$ at GCE in ionic liquid systems such as 1-methyl-3-ethylimidazolium chloride (EMIC) and 1-ethyl-3-methylimidazolium tetrafluoroborate ($EMIBF_4$).[21,22]

FE-SEM and EDS Characterization of Gold Deposits. Figures 2(a)-(c) shows the typical FE-SEM images of the Au deposited on FTO for 25, 50, or 100 s. The average size of Au deposits increased with deposition time (τ) (*ca.* 300, 500, and 1000 nm, respectively), and they were homogeneously distributed. The EDS spectrum confirmed the formation of pure Au by electrochemical deposition (Fig. 2(d)).

Voltammetric and EIS Characterization of Au/FTO Electrodes. The CVs of the Au/FTO electrodes in PBS (pH 7.0) over a potential range from 0.0 to 1.4 V clearly indicate the formation of gold oxide (AuO_x) on Au deposit, peaked at *ca.* 1.0 V by positive polarization,[23] which reduced back at *ca.* 0.4 V during the reverse scan (Fig. 3(a)). It was seen that both peaks reach a maximum current at the deposition time (τ) of 50 s, and thereafter decrease with τ. The latter behavior is attributable to a decrease in the net surface area of Au on FTO as the electrochemical deposition process continued. It is consistent with the monotonic increase in the size of Au nanostructures with increasing τ while the density decreased, as shown in the SEM images. This strongly suggested that the electrochemical deposition of Au on FTO was done by instantaneous nucleation process followed by the growth and coalescence of the existing nuclei without the formation of additional nuclei as suggested in the previous literatures.[20,24,25] Both CVs and EIS spectra in Figures 3(b) and 3(c) showed that the peak-to-peak separation (ΔE_p) and the charge transfer resistance (R_{ct}) were smallest at τ = 50 s. It indicated the highest electrochemical catalytic reactivities for Au/FTO prepared at τ = 50 s (Table 1), which was con-

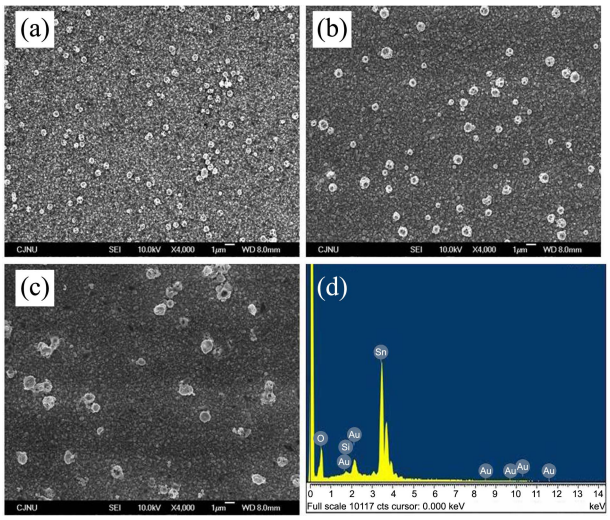

Figure 2. FE-SEM images of sub-micrometer size Au deposited on FTO for 25 s (a), 50 s (b), 100 s (c), and an EDS spectrum of the Au/FTO electrode deposited for 50 s (d).

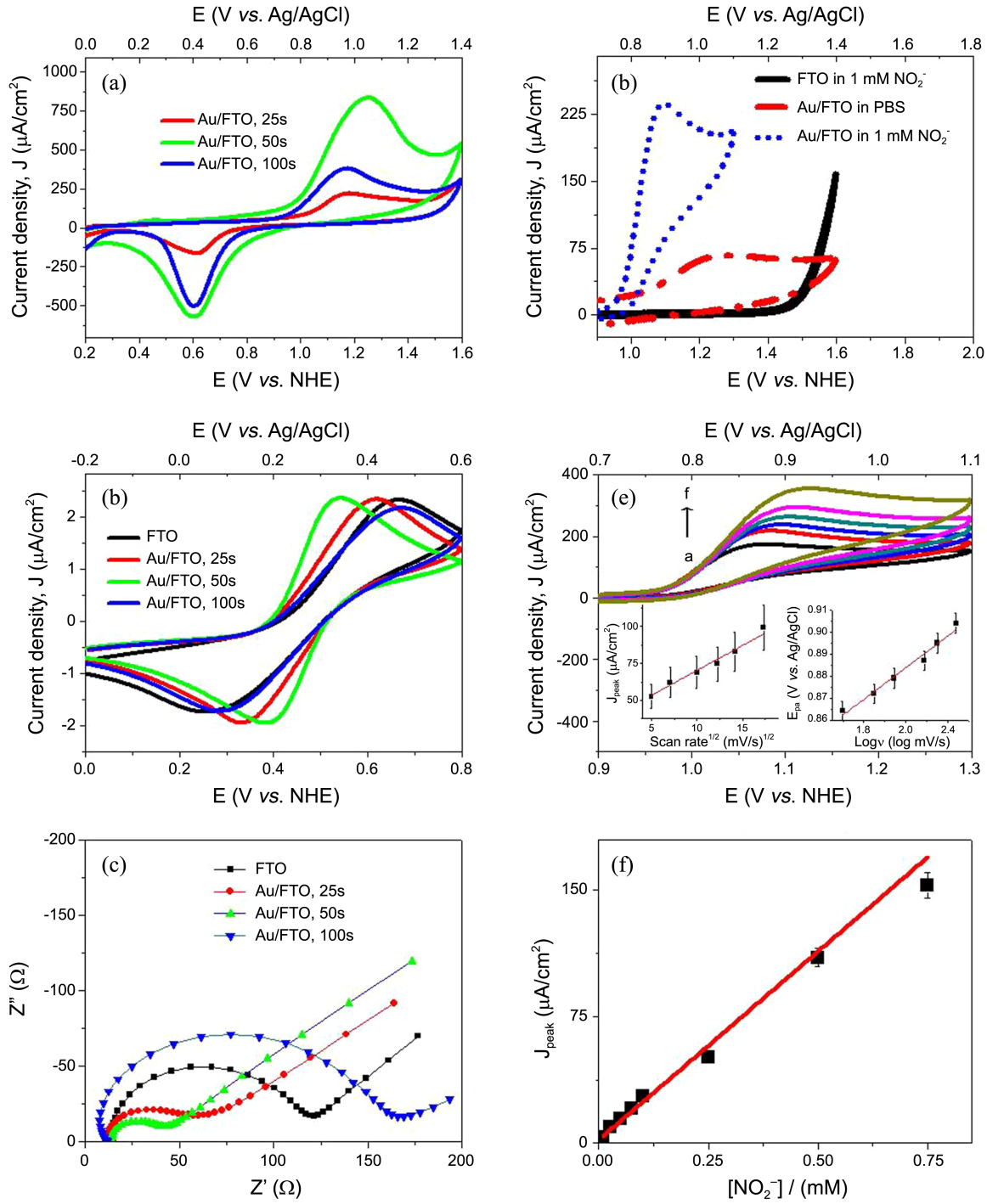

Figure 3. (a) Cyclic voltammograms (CVs) of FTO and different Au/FTO electrodes in PBS (pH 7.0): scan rate 100 mV·s^{-1}. CVs (b) and electrochemical impedance spectra (EIS) (c) of FTO and different Au/FTO electrodes in 5 mM $[Fe(CN)_6]^{3-/4-}$ (in PBS, pH 7.0); scan rate 100 mV·s^{-1}. (d) CVs of the Au/FTO electrode in 1 mM NO_2^- and PBS (pH 7.0), and FTO electrode in 1 mM NO_2^-; scan rate 100 mV·s^{-1}. (e) CVs of the Au/FTO electrode in 1 mM NO_2^- at different scan rates (a-f: 20, 50, 100, 150, 200, 300 mV·s^{-1}). Inset show the plot of J_{peak} *vs.* $\nu^{1/2}$ and E_{pa} *vs.* logν. (f) Calibration plot of J_{peak} *vs.* $[NO_2^-]$ (0.01, 0.025, 0.050, 0.075, 0.1, 0.25, 0.5 and 0.75 mM) obtained from differential pulse voltammetric responses at Au/FTO sensor.

sidered as the optimum condition hereafter, due to the maximized net surface area of Au under this deposition time. The net surface area of Au nanostructure on FTO was calculated from the net charge of the gold oxide (AuO_x) reduction with respect to that of the AuO_x monolayer (*ca.* 400 μC·cm^{-2}).[27,28] It reached to the maximum value up to *ca.* 0.13 cm^2, equivalent to *ca.* 40.6% of the geometric area of FTO, under optimum deposition time (50 s) as shown in Figure 3(a) (Table 1). The apparent standard heterogeneous rate constant (k_{app}) at the electrodes, calculated from EIS in Figure 3(c), also consistent with the trend observed in voltammograms and R_{ct} (Table 1).

Table 1. Electrochemical properties of FTO and Au/FTO electrodes

Electrodes	τ/s	Average particle size/nm	Surface area /cm^2	R_{ct}/Ω	Apparent standard heterogeneous rate constant (k_{app})[a]/cm·s^{-1}
FTO	-	-	-	110.15	4.4×10^{-9}
Au/FTO	25	~300	0.03	55.25	8.8×10^{-9}
Au/FTO	50	~500	0.13	35.55	1.4×10^{-8}
Au/FTO	100	~1000	0.07	162.85	3.0×10^{-9}

[a]k_{app} values were measured according to the previously reported method.[26]

Electrochemical Behavior of Nitrite at Au/FTO. Under the optimized condition, the Au/FTO electrode showed a well-defined oxidation wave in CV at *ca.* 0.89 V for 1 mM NO_2^- in PBS (pH 7.0), while there is no significant electrochemical reactivity of NO_2^- at the bare FTO electrode (Fig. 3(d)). The linear relationship between the NO_2^- oxidation peak current density and the square root of the scan rate ($\nu^{1/2}$) indicates that the NO_2^- oxidation is a diffusion-controlled process (Inset, Fig. 3(e)). The transfer coefficient (α) for NO_2^- oxidation is estimated to be 0.58 by assuming that the number of electrons (n_a) involved with the rate-limiting process is one, as obtained from the linear relationship between E_{pa} *vs.* log ν (Inset, Fig. 3(e)), which is evidenced by Eq. (1)[5], where *T*, *R*, and *F* are the temperature, gas, and Faraday constant, respectively.

$$E_{pa} = \left[\frac{2.3RT}{2(1-\alpha)n_a F}\right]\log \nu + K \quad (1)$$

The value of α, bigger than 0.5 in this case, implied that the relatively high catalytic oxidation rate of NO_2^- to NO_2 on Au was followed by the disproportionation reaction of NO_2, as shown in reactions (3) and (4), respectively.[29,30]

$$NO_2^- \rightarrow NO_2 + e^- \quad (3)$$

$$2NO_2 + H_2O \leftrightarrow NO_2^- + NO_3^- + 2H^+ \quad (4)$$

Analytical Performance of the Au/FTO Sensor. The sensitivity and the detection limit (*S/N* = 3) are estimated to be *ca.* 223.4 μA·cm^{-2}·mM^{-1} and 2.95 μM, respectively. They were calculated from the linear relationship between NO_2^- oxidation peak current densities (J_{peak}'s), obtained from differential pulse voltammetric (DPV) responses *vs.* [NO_2^-] in the range 10.0–7.5 × 10^2 μM (Fig. 3(f)). Thus, this electrode is highly reliable and appropriate for the real-time monitoring of NO_2^- to comply with the MCL of NO_2^-, as defined by the EPA. The average recovery of known spiked [NO_2^-] (20 μM) was in the range 97–102% for real samples including orange juice, grape juice, and local tap water (Table 2). The detection of NO_2^- at concentrations of up to 1 mM by this electrode was not affected by most of the common interfering species such as Cl^-, SO_4^{2-}, NO_3^-, CO_3^-, Ca^{2+}, Mg^{2+}, Zn^{2+}, and Na^+.

Table 2. Recovery results for NO_2^- detection in different real samples

Samples	NO_2^- added (μM)	NO_2^- found (μM)[a]	Recovery (%)
Tap water	20	20.40	102%
Grape Juice	20	19.8	99%
Orange Juice	20	19.4	97%

[a]average of three measurements

Conclusions

Homogeneous distributions of sub-micrometer size Au deposits on FTO (Au/FTO) were prepared by potential-step methods for detecting NO_2^-. It was found that the electrochemical deposition of Au on FTO occurred by instantaneous nucleation followed by the growth and coalescence of the existing nuclei. The Au/FTO electrode showed an improved electrocatalytic activity toward the oxidation of NO_2^- under the optimal conditions, with detection limit and sensitivity of 2.95 μM and 223.4 μA·cm^{-2}·mM^{-1}, respectively. There was a significant recovery ratio from real samples, and no significant interference was observed from the common interfering ions. Based on the electrochemical analysis, it was found that a relatively high rate of catalytic oxidation of NO_2^- to NO_2 occurred at Au surface and was followed by a disproportionation reaction of NO_2 to NO_2^- and NO_3^-.

Acknowledgments. This research was supported by Basic Science Research Program through the National Research Foundation of Korea (NRF) funded by the Ministry of Education (2013R1A1A4A01013236) and by the New & Renewable Energy Core Technology Program of the Korea Institute of Energy Technology Evaluation and Planning (KETEP) granted financial resource from the Ministry of Trade, Industry & Energy, Republic of Korea (No. 20133030000140).

References

1. Saha, K.; Agasti, S. S.; Kim, C.; Li, X.; Rotello, V. M. *Chem. Rev.* **2012**, *112*, 2739.
2. Kumar, S.; Zou, S. *J. Phys. Chem. B* **2005**, *109*, 15707.
3. Yu, C.; Guo, J.; Gu, H. *Electroanalysis* **2010**, *22*, 1005.
4. Focazio, M. J.; Tipton, D.; Shapiro, S. D.; Geiger, L. H. *Ground Water Monit. Remediat.* **2006**, *26*, 92.
5. Cui, Y.; Yang, C.; Zeng, W.; Oyama, M.; Pu, W.; Zhang, J. *Anal. Sci.* **2007**, *23*, 1421.
6. Li, S.-J.; Zhao, G.-Y.; Zhang, R.-X.; Hou, Y.-L.; Liu, L.; Pang, H. *Microchim. Acta* **2013**, *180*, 821.
7. Choi, K. K.; Fung, K. W. *Analyst* **1980**, *105*, 241.
8. Ahammad, A. J. S.; Rahman, M. M.; Xu, G.-R.; Kim, S.; Lee, J.-J. *Electrochim. Acta* **2011**, *56*, 5266.

9. Kim, Y. J.; Rahman, M. M.; Lee, J.-J. *Sens. Actuator B-Chem.* **2013**, *177*, 172.
10. Rahman, M. M.; Ahammad, A. J. S.; Jin, J.-H.; Ahn, S. J.; Lee, J.-J. *Sensors* **2010**, *10*, 4855.
11. Lee, S. H.; Field, L. R. *Anal. Chem.* **1984**, *56*, 2647.
12. Huang, X.; Li, Y.; Chen, Y.; Wang, L. *Sens. Actuator B-Chem.* **2008**, *134*, 780.
13. Margalith, T.; Buchinsky, O.; Cohen, D. A; Abare, A. C.; Hansen, M.; DenBaars, S. P.; Coldren, L. A. *Appl. Phys. Lett.* **1999**, *74*, 3930.
14. Ahammad, A. J. S.; Choi, Y.-H.; Koh, K.; Kim, J. H.; Lee, J.-J.; Lee, M. *Int. J. Electrochem. Sci.* **2011**, *6*, 1906.
15. Rahman, M. M.; Nath, N. C. D.; Noh, K.-M.; Kim, J.; Lee, J.-J. *Int. J. Photoenergy* **2013**, *2013*, Article ID 563170.
16. Cheng, W.; Han, X.; Wang, E.; Dong, S. *Electroanalysis* **2004**, *16*, 127.
17. Wang, L.; Mao, W.; Ni, D.; Di, J.; Wu, Y.; Tu, Y. *Electrochem. Commun.* **2008**, *10*, 673.
18. Dai, X.; Compton, R. G. *Anal. Sci.* **2006**, *22*, 567.
19. Sakai, N.; Fujiwara, Y.; Arai, M.; Yu, K.; Tatsuma, T. *J. Eletroanal. Chem.* **2009**, *628*, 7.
20. Sheridan, E.; Hjelm, J.; Forster, R. J. *J. Eletroanal. Chem.* **2007**, *608*, 1.
21. Xu, X.-H.; Hussey, C. L. *J. Electrochem. Soc.* **1992**, *139*, 3103.
22. Oyama, T.; Okajima, T.; Ohsaka, T. *J. Electrochem. Soc.* **2007**, *154*, D322.
23. Yu, A.; Liang, Z.; Cho, J.; Caruso, F. *Nano Lett.* **2003**, *3*, 1203.
24. Lee, J.-J.; Bae, I. T.; Scherson, D. A.; Miller, B.; Wheeler, K. A. *J. Electrochem. Soc.* **2000**, *147*, 562.
25. Lee, J.-J.; Miller, B.; Shi, X.; Kalish, R.; Wheeler, K. A. *J. Electrochem. Soc.* **2001**, *148*, C183.
26. Zhang, J.; Oyama, M. *Anal. Chim. Acta* **2005**, *540*, 299.
27. El-Deab, M. S.; Sotomura, T.; Ohsaka, T. *J. Electrochem. Soc.* **2005**, *152*, C1.
28. Dai, X.; Nekrassova, O.; Hyde, M. E.; Compton, R. G. *Anal. Chem.* **2004**, *76*, 5924.
29. Soderberg, J. N.; Co, A. C.; Sirk, A. H. C.; Birss, V. I. *J. Phys. Chem. B* **2006**, *110*, 10401.
30. Guidelli, R.; Pergola, F.; Raspi, G. *Anal. Chem.* **1972**, *44*, 745.